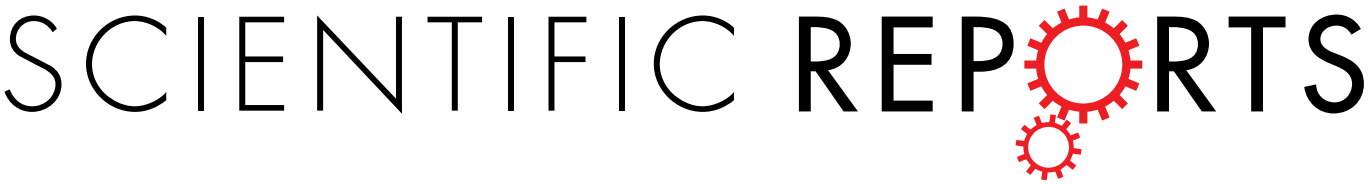

OPEN

Chemical ordering in substituted fluorite oxides: a computational investigation of $Ho_2Zr_2O_7$ and $RE_2Th_2O_7$ (RE=Ho, Y, Gd, Nd, La)

Received: 30 August 2016
Accepted: 10 November 2016
Published: 12 December 2016

Jonathan M. Solomon[1], Jacob Shamblin[2,3], Maik Lang[2], Alexandra Navrotsky[4] & Mark Asta[1]

Fluorite-structured oxides find widespread use for applications spanning nuclear energy and waste containment, energy conversion, and sensing. In such applications the host tetravalent cation is often partially substituted by trivalent cations, with an associated formation of charge-compensating oxygen vacancies. The stability and properties of such materials are known to be influenced strongly by chemical ordering of the cations and vacancies, and the nature of such ordering and associated energetics are thus of considerable interest. Here we employ density-functional theory (DFT) calculations to study the structure and energetics of cation and oxygen-vacancy ordering in $Ho_2Zr_2O_7$. In a recent neutron total scattering study, solid solutions in this system were reported to feature local chemical ordering based on the fluorite-derivative weberite structure. The calculations show a preferred chemical ordering qualitatively consistent with these findings, and yield values for the ordering energy of 9.5 kJ/mol-cation. Similar DFT calculations are applied to additional $RE_2Th_2O_7$ fluorite compounds, spanning a range of values for the ratio of the tetravalent and trivalent (RE) cation radii. The results demonstrate that weberite-type order becomes destabilized with increasing values of this size ratio, consistent with an increasing energetic preference for the tetravalent cations to have higher oxygen coordination.

Fluorite-structured oxide compounds have been actively investigated for a range of technological applications, spanning solid-state ion conductors in electrochemical devices, to wasteforms and fuels for nuclear energy. In many such applications, the host tetravalent cations are substituted to varying degrees with trivalent cations such as rare earth (RE) atoms, which are charge-compensated by oxygen vacancies. Such substitutions can lead to the formation of configurationally long-range-ordered structures, such as pyrochlores[1] or the δ-$Zr_3Y_4O_{12}$ phase[2], or disordered fluorite solid solutions that can be thermodynamically stable over extended composition ranges[3]. In the latter case, although configurational long-range order is absent on the cation and anion sublattices, experimental studies based on advanced structural characterization and thermochemistry techniques (e.g., refs 4–8 and references therein) have documented in several systems the presence of significant short-range order, i.e., local association and clustering of the different ionic species and oxygen vacancies. These experimental studies have been augmented by atomic-scale computational investigations (e.g., refs 9–16 and references therein), which have established preferred structural motifs and associated energetic driving forces for defect association and compositional ordering across a broad range of chemistries.

The interest in chemical ordering in trivalent-substituted fluorite oxide solid solutions stems from its effects on the stability and physical properties of these materials. For example, short-range ordering significantly influences the overall energetic stability of yttria stabilized zirconia[4], and it is expected to be similarly important to the phase stability of other related solid solutions more generally[8]. Further, the tendency for oxygen vacancies to bind preferentially to either the host or trivalent cation reduces the mobility of oxygen ions, which can be detrimental for performance in fuel cell electrolyte and oxygen sensor applications[17], while it is believed to reduce oxidative

[1]Department of Materials Science and Engineering, University of California Berkeley, Berkeley, CA 94720, United States. [2]Department of Nuclear Engineering, University of Tennessee, Knoxville, Tennessee 37996, United States. [3]Department of Physics and Astronomy, University of Tennessee, Knoxville, Tennessee 37996, United States. [4]Peter A. Rock Thermochemistry Laboratory and NEAT ORU, University of California Davis, Davis, CA 95616, United States. Correspondence and requests for materials should be addressed to M.A. (email: mdasta@berkeley.edu)

corrosion rates in spent nuclear fuel[18,19]. Given the importance of these issues, detailed characterization of the nature, degree and spatial extent of short-range order in fluorite solid solutions is of considerable interest for the development of fluorite-structured oxides across a variety of applications.

In a very recent contribution, pair distribution function (PDF) analysis based on neutron total scattering measurements for the RE-substituted fluorite oxide system $Ho_2Zr_2O_7$ has provided new insights into the nature of structural ordering[20]. In this study, the diffraction patterns for the samples studied displayed only peaks characteristic of the fluorite structure, indicative of the stability of a disordered fluorite solid-solution phase, consistent with previous reports (see, e.g., Stanek *et al.*[21] and references therein). Nevertheless, the PDF analysis led to the conclusion that pronounced local structural ordering is present. Further, it was concluded that this local order can be described as being based on a weberite type fluorite-derivative superstructure. This discovery is particularly interesting in the context of previous investigations of the energetic stability of pyrochlore ordering in related systems with $A_2B_2O_7$ compositions[1], which have established that pyrochlore phases are stable when the ratio of the radius of the B^{4+} to A^{3+} cations is in the range of 0.56 to 0.68. For $Ho_2Zr_2O_7$ the value of this ratio is significantly larger, at 0.83, and the observation of local short-range order of weberite type in this compound raises the question of whether this ordering may be found more generally in other RE-substituted systems with even larger tetravalent cations. Specifically, the possible relevance of weberite-type ordering for the structure of disordered fluorite phases observed in RE-substituted actinide-based fluorite solid solutions is of significant interest due to the potential importance for the stability and properties of nuclear fuel and wasteform materials.

In the present study we investigate these issues employing first-principles density-functional-theory (DFT) calculations. Specifically, we investigate the nature of the preferred fluorite-derivative structural ordering in $Ho_2Zr_2O_7$, and calculate values for the energetic driving force underlying its formation, through the consideration of a set of hypothetical long-range-ordered configurations designed to probe energetically-preferred ordering motifs. We further show that the stability of the weberite-type ordering reported in ref. 20 is strongly influenced by the ratio of cation radii, by comparing the configurational energetics in $Ho_2Zr_2O_7$ with those in RE-substituted ThO_2 systems (RE=Ho, Y, Gd, Nd, and La) with the same stoichiometry. The focus on ThO_2 host materials, which have received growing attention as fuel materials for nuclear energy production[18,19], is motivated in part by the fact that this system provides access to larger ratios of the radii for the host tetravalent to the substituted RE trivalent cation. Further, although these systems are known to form disordered fluorite phases rather than ordered fluorite-derivative compounds under experimentally realized synthesis conditions (see, e.g., Aizenshtein *et al.*[22] and references therein), previous calorimetric[22] and computational[15] studies have concluded that the thermodynamic stability of RE doped ThO_2 solid solutions are influenced by short range ordering that varies with the size of the trivalent RE cation. A comparison of the DFT results presented here for both $Ho_2Zr_2O_7$ and the $RE_2Th_2O_7$ compounds shows a systematic trend for the weberite-type structural ordering reported in ref. 20 to be energetically destabilized with increasing ratio of the tetravalent to trivalent cation size.

Results and Discussion

Chemical ordering in $Ho_2Zr_2O_7$. Motivated by the recent experimental observations reported by Shamblin *et al.*[20], we begin by considering the energetics associated with the ordering of the Ho and Zr cations, and oxygen ions and vacancies, over the cation and anion sublattices of the fluorite structure for $Ho_2Zr_2O_7$. Employing DFT calculations, as described in the Methods section, we compute the energetics for different cation and anion arrangements on the fluorite lattice, considering three different classes of configurations.

The first set of configurations consists of all arrangements that can be generated as superstructures of the fluorite structure based on unit cells containing 2 tetravalent cations, 2 trivalent cations, 7 oxygen ions and 1 oxygen vacancy. Using a structural enumeration algorithm[23] implemented in the Alloy Theoretic Automated Toolkit (ATAT)[24,25], we find 27 possible configurations, which will be referred to in what follows as "$A_2B_2O_7$-fluorite" configurations. We note that this set of enumerated configurations does not include the pyrochlore structure, which has a larger unit cell; pyrochlore ordering was not explicitly considered in this work as it is known to be energetically stable for B^{4+}/A^{3+} size ratios smaller than those for $Ho_2Zr_2O_7$ (see the Introduction section). We further note that although each of these is derived from different arrangements of Ho, Zr, oxygen and vacancies over the sublattices of the fluorite structure, the compositional ordering breaks the cubic symmetry such that the 27 configurations display a range of space group symmetries. As an example of the structures generated by this procedure we show in Fig. 1 two of the enumerated $A_2B_2O_7$-fluorite configurations, which correspond to the lowest (A) and highest (B) energy structures obtained from DFT calculations for $Ho_2Zr_2O_7$. Figure 1 illustrates that the structures correspond to different ordering patterns of the cations and oxygen vacancies. It is worth clarifying that the "$A_2B_2O_7$-fluorite" structures should not be misinterpreted as disordered "defect fluorite"; rather, they represent ordered superstructures of fluorite.

The second set of compositional arrangements considered are those associated with the weberite-type structure reported by Shamblin *et al.*[20]. Specifically, following ref. 20, we consider a conventional 44-atom unit cell based on the Ccmm space group, with Zr and Ho cations occupying the 4*a* and 4*b* sites, respectively, and sharing occupancy of the 8*g* sites. Oxygen ions fully occupy the 16*h* site, while three separate 4*c* sites are occupied by oxygen ions, and the fourth 4*c* site is vacant. The specific positions of the oxygen vacancies give rise to a structure in which the Ho atoms on the 4*b* sites are coordinated by 8 nearest-neighbor oxygen ions, the Zr atoms on the 4*a* site are coordinated by 6 oxygen ions, and the cations on the mixed 8*g* sites each have 7-fold coordination. In order to determine the most energetically stable weberite-type configuration based on this structure, we generate 70 (=$C(8, 4)$) configurations consisting of all possible arrangements of the four B^{4+} ions and four A^{3+} ions on the 8*g* sites, which we will refer to in what follows as "weberite-type" configurations. As an example of the structures generated by this procedure we show in Fig. 2 two of the weberite-type configurations, which correspond to the lowest (A) and highest (B) energy structures obtained from DFT calculations for $Ho_2Zr_2O_7$. It should be noted that both the "weberite-type" and "$A_2B_2O_7$-fluorite" configurations can be categorized as fluorite superstructures,

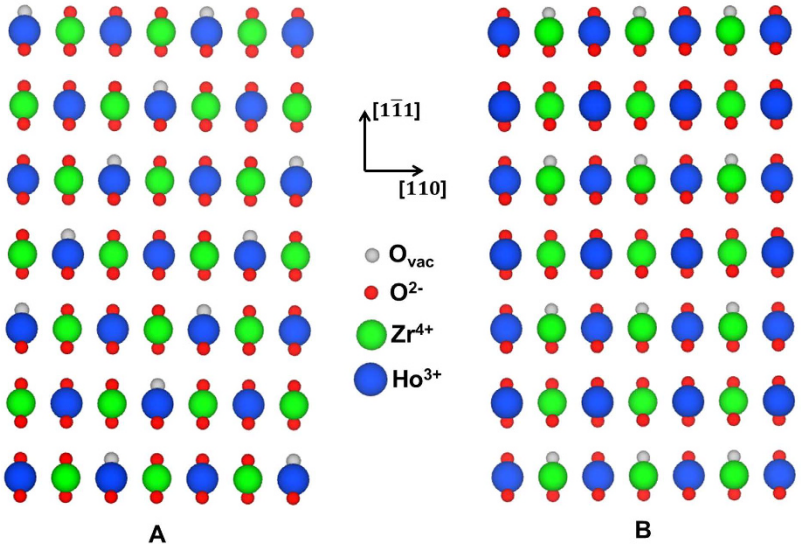

Figure 1. Projections of the lowest (**A**) and highest (**B**) energy $A_2B_2O_7$-fluorite configurations for $Ho_2Zr_2O_7$. Projections are shown along the ⟨211⟩ direction. For clarity, the ions are shown in their unrelaxed fluorite positions, and oxygen vacancies (denoted as O_{vac}) are represented by gray circles.

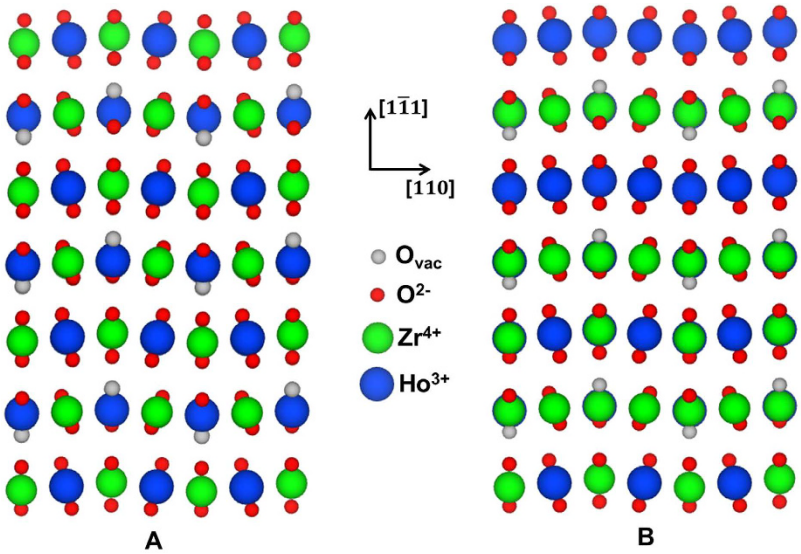

Figure 2. Projections of the lowest (**A**) and highest (**B**) energy weberite-type configurations for $Ho_2Zr_2O_7$. Projections are shown along the ⟨211⟩ direction. For clarity, the ions are shown in their unrelaxed weberite positions, and oxygen vacancies (denoted as O_{vac}) are represented by gray circles.

and the distinction between them made here is purely for computational reasons, associated with the fact that they were generated by structural enumeration considering different constraints on the possible superstructure unit cells.

The third set of configurations considered in the calculations are so-called special-quasirandom structures (SQS)[26]. The SQS considered here are designed to be a periodic superstructure of fluorite with the atomic configuration of the B^{4+}, A^{3+}, oxygen and vacancy ions chosen to give short-ranged pair and multibody correlation functions matching as closely as possible those of a material with ideal, statistically random substitutional disorder on the cation and anion sublattices. The SQS structures are considered as they provide a means for computing from periodic-DFT calculations the energy of a phase with ideal random cation and anion distributions. The differences in energy between the SQS structures and the ordered configurations described above thus provide an estimate of the so-called "ordering energy," which gives the energetic driving force for configurational ordering on the underlying parent (fluorite) structure. We consider two different SQS models taken from the literature[27,28], one containing 297 atoms and the other 88 atoms. The former was shown by Wolff-Goodrich *et al.*[28] to give more accurate estimates of the random phase energy, but it is significantly more computationally expensive than the

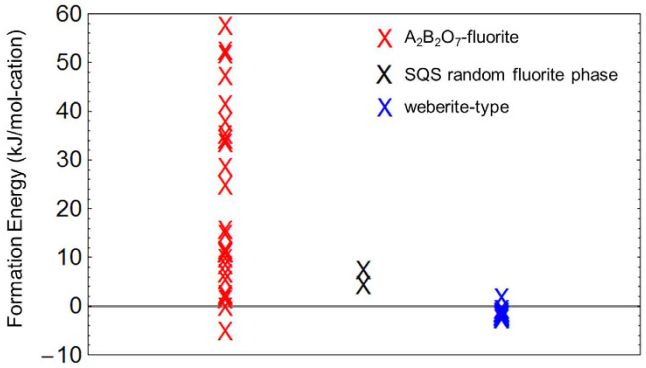

Figure 3. Formation energies (kJ/mol-cation) of all enumerated structures. $A_2B_2O_7$-fluorite, weberite-type configurations, and the 88 atom ($\Delta H_f = 7.2$ kJ/mol-cation) and 297 atom ($\Delta H_f = 4.0$ kJ/mol-cation) SQS models of a random fluorite phase for $Ho_2Zr_2O_7$ are shown.

B^{4+}	A^{3+}	ΔH_f (kJ/mol-cation) $A_2B_2O_7$-fluorite	ΔH_f (kJ/mol-cation) weberite	ΔH_f (kJ/mol-cation) Difference	B^{4+}/A^{3+} Size Ratio
Zr	Ho	−5.4	−2.6	2.8	0.828
Th	La	9.1	13.5	4.4	0.905
Th	Nd	7.9	20.0	12.1	0.947
Th	Gd	12.5	37.4	24.9	0.997
Th	Y	14.8	43.3	28.5	1.030
Th	Ho	15.2	46.5	31.3	1.034

Table 1. Formation energies (kJ/mol-cation) for the lowest-energy fully relaxed $A_2B_2O_7$-fluorite and weberite-type configurations. "ΔH_f difference" denotes the difference between the $A_2B_2O_7$-fluorite and weberite-type formation energies ("ΔH_f $A_2B_2O_7$-fluorite" and "ΔH_f weberite").

latter. Therefore, the smaller 88-atom SQS is included because it will be used as the basis for exploring energetic trends in the next section.

The DFT calculated energies for all enumerated weberite-type, $A_2B_2O_7$-fluorite, and SQS configurations for $Ho_2Zr_2O_7$ are shown in Fig. 3. The results are presented as formation energies (ΔH_f) with respect to constituent binary oxides, defined as follows for an $A_2B_2O_7$ structure, with A and B denoting the trivalent and tetravalent cations, respectively:

$$\Delta H_f = E(A_{0.5}B_{0.5}O_{1.75}) - 0.5E(BO_2) - 0.5E(AO_{1.5}) \quad (1)$$

where the energies E and ΔH_f are defined per mole of cations. With this definition, positive values of ΔH_f indicate an energetic preference for phase separation into constituent binary oxides, while negative values indicate that the ordered configurations are stable with respect to phase separation and suggest an energetic tendency towards compound formation.

We start by considering the formation energy of the ideal random phase, which is predicted to be positive, with values of $\Delta H_f = 7.2$ and 4.0 kJ/mol-cation for the 88 and 297 atom SQS models, respectively. Thus, the SQS models predict that an ideal random fluorite phase for $Ho_2Zr_2O_7$ would have a positive enthalpy of formation, and would be unstable with respect to phase separation to the constituent binary oxides at low temperatures, but could be stabilized by its configurational entropy at high temperatures. Considering next the results for the different ordered configurations, it can be seen that the different weberite-type configurations are calculated to be very close in energy, which is not surprising since the nearest-neighbor oxygen coordination numbers around each cation are identical for each of the different structures (see above). By contrast, the spread in energy for the $A_2B_2O_7$ fluorite configurations is much larger, as the structures generated in the enumeration approach include some atomic arrangements that are electrostatically very unfavorable. Importantly, it is found that the lowest energy $A_2B_2O_7$-fluorite and weberite-type configurations have *negative* formation energies, in contrast to what was found for the ideal random phase (as modeled by the SQS structures). The results thus show that configurational ordering lowers the energy and leads to the energetic stabilization of $Ho_2Zr_2O_7$ fluorite-derivative structures relative to phase separation to the constituent binary oxides. Taking the 297-atom SQS value as the best estimate for the formation energy of the ideal random solid phase, the calculations predict ordering energies of 9.5 and 6.7 kJ/mol-cation for the lowest energy $A_2B_2O_7$-fluorite and weberite-type configurations, respectively.

The formation energies of the lowest-energy $A_2B_2O_7$-fluorite and weberite-type configurations of $Ho_2Zr_2O_7$ composition are shown in the top row of Table 1. It can be seen that ΔH_f for the lowest-energy $A_2B_2O_7$-fluorite configuration is slightly lower (i.e., the structure is energetically more stable) than that found for the lowest-energy weberite-type configuration, by approximately 3 kJ/mol-cation. This DFT result may seem at odds with the

	Zr	Th	Ho	Y	Gd	Nd	La
Charge	4+	4+	3+	3+	3+	3+	3+
Size (Å)	0.84	1.05	1.015	1.019	1.053	1.109	1.16

Table 2. Charges and sizes of cations considered in this work. The sizes represent Shannon eightfold-coordination ionic radii[34].

conclusion of Shamblin *et al.*[20] that the local order in the $Ho_2Zr_2O_7$ is of weberite type, since we are finding another configuration with lower energy. However, despite their different space-group symmetries, the configurational arrangement of the atoms for the lowest-energy $A_2B_2O_7$-fluorite configuration is in fact very similar to what is found for the lowest-energy weberite-type configuration. It was found through simulations of the PDFs that both the $A_2B_2O_7$-fluorite and weberite-type configurations lead to a comparable level of agreement with the experimental data reported in ref. 20, such that the difference in ordering is expected to be too subtle to distinguish from the neutron total scattering analysis.

The similarity of the lowest-energy $A_2B_2O_7$-fluorite and weberite-type configurations can be appreciated by comparing their projected images shown in Figs 1(A) and 2(A), respectively. Both are seen to show identical "checkerboard" configurations for the Ho and Zr cations in this projection, and display exactly the same ordering of the cations over the sites of the fluorite lattice. Note that the lowest-energy $A_2B_2O_7$-fluorite configuration is relaxed and therefore more distorted from what is shown in the figure, tending towards the lower-symmetry, weberite-type ordering as well. The primary difference between the two structures is seen to be associated with the ordering of the oxygen vacancies. Specifically, the oxygen vacancies in the lowest-energy $A_2B_2O_7$-fluorite configuration are ordered as second nearest neighbors along the ⟨110⟩ direction in the lowest-energy $A_2B_2O_7$-fluorite configuration, whereas for the lowest-energy weberite-type configuration they are ordered as third nearest neighbors along ⟨111⟩. This difference in vacancy ordering is relatively subtle, as the number of nearest-neighbor oxygen ions around Zr is identical in both structures. Specifically, both structures feature the same preference for Zr (Ho) to be surrounded by less (more) oxygen ions in its nearest-neighbor shell than the average concentration. In both the lowest-energy $A_2B_2O_7$-fluorite and weberite-type structures the average number of oxygen ions surrounding Zr (Ho) is 6.5 (7.5), compared to the number of 7 that would characterize a random distribution. This preference for lower (higher) coordination around the B^{4+} (A^{3+}) cation is consistent with reverse Monte Carlo (RMC) analysis from neutron total scattering[7] and X-ray absorption experiments[29,30] on zirconate and hafnate systems (i.e., $A_2B_2O_7$, B=Zr, Hf), with a general trend towards increasing (decreasing) oxygen ion coordination of B (A) as the A cation size decreases (this trend is discussed in further detail in the next section). Similar coordination behavior was also found for titanate systems[31]; however, the local order was found to be pyrochlore, which is distinctly different compared to the preferred weberite-type configuration found here and in ref. 29 for $Ho_2Zr_2O_7$ (a comparison of the local order for pyrochlore and weberite-type configurations is included in the next section).

Chemical ordering and relative stability of weberite-type structures in $RE_2Th_2O_7$. In this section we consider the results obtained by applying the computational approach described above to the study of the energetics of chemical ordering in $RE_2Th_2O_7$ systems, where the trivalent RE cations considered are listed along with their sizes relative to tetravalent Zr and Th in Table 2. We chose thorium as a representative actinide element because it has only one oxidation state (4+) and no *f*-electrons to complicate the DFT calculations. For each choice of RE trivalent cation we performed DFT calculations to identify the lowest-energy $A_2B_2O_7$-fluorite and weberite-type configurations from amongst the enumerated structures described in the previous section. The formation energies for these lowest-energy structures are listed in Table 1, and are plotted in Fig. 4, along with the corresponding values for the 88-atom SQS structure (approximating a random fluorite phase), as a function of the ratio of the tetravalent to trivalent cation ionic radius (referred to hereafter at the B^{4+}/A^{3+} size ratio). The results for $Ho_2Zr_2O_7$ are also included in Fig. 4 for comparison.

Figure 4 displays clear trends with increasing values of the B^{4+}/A^{3+} size ratio. First, all of the ΔH_f values calculated in the $RE_2Th_2O_7$ systems are positive, with a magnitude that tends to increase with increasing value of the B^{4+}/A^{3+} size ratio. In other words, the fluorite-derivative structures considered here for $RE_2Th_2O_7$ are found to become increasingly unstable, with respect to phase separation to constituent binary oxides, as the size of the trivalent RE cation decreases. This trend is consistent with the analysis of previous DFT and calorimetric studies on similar defected fluorite oxide systems given by Zhang *et al.*[32]. The general trend can be rationalized based on simple ionic coordination arguments. Specifically, tetravalent (trivalent) cations tend to reduce (increase) the nearest-neighbor oxygen ion coordination relative to the constituent binary oxides upon mixing, and therefore systems with smaller (larger) B^{4+} (A^{3+}) cations are expected to be more energetically stable. The net effect is that, amongst the systems considered in this work, only for $Ho_2Zr_2O_7$, where the B^{4+}/A^{3+} size ratio has the minimum value of 0.828, do the fluorite-derivative structures have negative formation energies and are thus energetically stable with respect to phase separation to constituent binary oxides. A negative formation energy for a similar system, $Y_2Zr_2O_7$, was calculated previously with a magnitude similar to $Ho_2Zr_2O_7$[11–13]. The effect of changing Zr to the larger Th cation is to destabilize these structures, to a degree that increases with decreasing size of the RE ion.

The second trend observed in Fig. 4 is the increasing difference between ΔH_f for the lowest-energy weberite-type and $A_2B_2O_7$-fluorite configurations with increasing B^{4+}/A^{3+} size ratio. While the energies for these two configurations are close for $Ho_2Zr_2O_7$, the weberite-type configurations become increasingly higher in energy than the lowest-energy $A_2B_2O_7$-fluorite configuration as the size of the RE ion decreases in the $RE_2Th_2O_7$ systems. The same trend is also apparent when comparing the energies of the weberite-type configurations with the SQS model of the ideal random phase: while the weberite-type configurations are lower in energy than the random

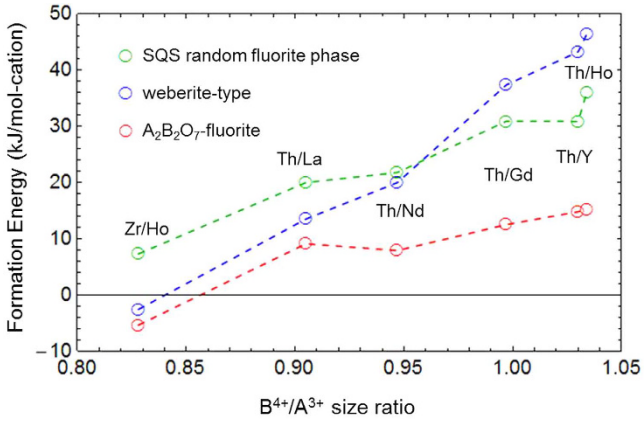

Figure 4. Formation energy vs. cation size ratio. Formation energies (kJ/mol-cation) of lowest-energy $A_2B_2O_7$-fluorite, lowest-energy weberite-type, and SQS random phase configurations (88 atom) as a function of B^{4+}/A^{3+} size ratio are plotted for $Ho_2Zr_2O_7$ and $RE_2Th_2O_7$ systems.

Structure	α_B
Pyrochlore	−0.14
weberite-type configuration	−0.07
Lowest-energy $A_2B_2O_7$ configuration for $Ho_2Zr_2O_7$	−0.07
δ-$Zr_3Y_4O_{12}$	−0.03
Ideal random fluorite phase	0
Lowest-energy $A_2B_2O_7$ configuration for $RE_2Th_2O_7$	0.07

Table 3. Short-range-order parameters α_B of the first nearest-neighbor anion shell. α_B is calculated based on the anion shell around tetravalent cations (B^{4+}) in pyrochlore, weberite-type, δ-$Zr_3Y_4O_{12}$, ideal random phase, and computed lowest-energy configurations for the $A_2B_2O_7$ systems considered in this work.

phase for smaller values of the B^{4+}/A^{3+} size ratio, they become higher in energy for larger size ratios. These overall trends can be understood based on a consideration of the oxygen neighbor coordinations around the different cation species in the different types of configurations, which is described next.

The weberite-type configurations all feature an average number of 7.5 oxygen neighbors surrounding the trivalent cation, and 6.5 oxygen neighbors surrounding the tetravalent cation (see the description of the weberite-type structure given in the previous section). By contrast, the lowest-energy $A_2B_2O_7$-fluorite configuration for $RE_2Th_2O_7$ (which is the same configuration for all of the RE elements considered) features a larger oxygen coordination surrounding tetravalent Th than the trivalent RE cations, namely 7.5 (6.5) oxygen neighbors surrounding the tetravalent (trivalent) cation. Recall that the random phase has the average number of 7 oxygen ions around both trivalent and tetravalent cations. Consistent with the coordination arguments summarized above, the DFT results suggest that while the larger oxygen coordination around the trivalent RE cation is favored energetically for the $Ho_2Zr_2O_7$ system, it is disfavored in the $RE_2Th_2O_7$ systems, due to the larger size of the Th cation relative to Zr, to a degree that increases with decreasing size of the RE ion.

To put the energy trends related to oxygen coordination into a broader context, we summarize the nature of the preferred compositional ordering in the current and related systems in Table 3. In this table, we report for the weberite-type structure, and lowest-energy $A_2B_2O_7$-fluorite type structures found here the preferred oxygen coordination number, as described through a short-range-order (SRO) parameter α_B. By analogy with the Warren-Cowley[33] parameter commonly used to describe SRO in alloys, we define α_B as follows:

$$\alpha_B = \frac{P_O^B}{C_O} - 1, \tag{2}$$

where P_O^B is the fraction of nearest-neighbor anion-sublattice sites surrounding a tetravalent B cation (Zr or Th in the current study) that are occupied by oxygen ions, while C_O is the average concentration (site fraction) of anion sublattice sites occupied by oxygen. For an $A_2B_2O_7$ fluorite phase with ideal random substitutional disorder, α_B is identically zero, and positive (negative) values indicate a preferential coordination of oxygen around tetravalent B (trivalent A) cations.

The results in Table 3 show positive and negative values for the lowest-energy $A_2B_2O_7$-fluorite configurations for $RE_2Th_2O_7$ and $Ho_2Zr_2O_7$, respectively, and negative values are associated with weberite-type configurations. Also included in Table 3 are values of α_B for pyrochlore and δ-$Zr_3Y_4O_{12}$ compounds, which are additional experimentally-observed fluorite-derivative structures featuring higher oxygen coordination around trivalent relative to tetravalent cations. It is well documented in the literature that pyrochlore systems are stable for

B^{4+}/A^{3+} size ratios smaller than those characteristic of the systems considered here[1] (c.f., the discussion in the Introduction section). It is perhaps not surprising that the δ-$Zr_3Y_4O_{12}$ phase and lowest-energy $A_2B_2O_7$ configuration for $Ho_2Zr_2O_7$ have a similar oxygen coordination preference (i.e., reduced (increased) oxygen coordination for the tetravalent (trivalent) cation relative to the random phase), given that the Ho and Y cations have similar ionic radii (1.015 and 1.019 Å, respectively[34]). Given this observation, and previous work by Stanek *et al.*[21] predicting stability of δ-phase structures for systems with cation size ratios bordering on those considered here, a more complete understanding of ordering tendencies in these systems would benefit from future work investigating the competition between δ-phase related ordering and the structures studied here for $A_2B_2O_7$ compositions. Overall, the results in Fig. 4 and Table 3 illustrate the trend that as the B^{4+}/A^{3+} size ratio increases from the small values characteristic of pyrochlore ordering to the much larger values characterizing the $RE_2Th_2O_7$ systems discussed in this section, there is an increasing preference for lowering the coordination of oxygen ions around the trivalent cation in favor of increasing the coordination around the tetravalent cation.

Summary and Conclusions

Density-functional-theory calculations have been undertaken to investigate the ordering energetics of tetravalent and trivalent cations and oxygen vacancies on fluorite-structured $Ho_2Zr_2O_7$ and $RE_2Th_2O_7$ (with RE=Ho, Y, Gd, Nd, and La). In these systems, formation energies were computed for a set of ordered $A_2B_2O_7$-fluorite derivative configurations, representing all possible arrangements of the tetravalent (B) and trivalent (A) cations and oxygen vacancies over the sites of the fluorite structure with 11-atom primitive unit cells, as well as a set of configurations enumerated by considering all possible cation arrangements over the mixing site of the weberite structure reported by Shamblin *et al.*[20]. For $Ho_2Zr_2O_7$, the results establish an energetic driving force for ordering on the fluorite lattice that is characterized by cation arrangements illustrated in Fig. 1(A), and a preference for a higher coordination of Ho by oxygen relative to Zr cations. The associated magnitude of the ordering energy is calculated to be approximately 9.5 kJ/mol-cation. The results are qualitatively consistent with the findings reported in the work of Shamblin *et al.*[20], in that the lowest-energy configuration obtained from the enumerated ordered fluorite superstructures of $A_2B_2O_7$ features the same type of cation ordering and the same average number of nearest-neighbor oxygen ions surrounding Ho and Zr as the lowest energy weberite configuration identified in the DFT calculations.

For the $RE_2Th_2O_7$ systems, the DFT calculations show that as the value of the B^{4+}/A^{3+} size ratio increases, there is a growing energetic preference for the tetravalent cation to have higher oxygen coordination relative to the trivalent cation. This leads to a destabilization of weberite-type order relative to ideally random phases and ordered configurations with higher average oxygen coordination around Th cations. A comparison of the lowest-energy configurations obtained here with those found in the long-range-ordered δ-$Zr_3Y_4O_{12}$ and pyrochlore phases, which are observed to be stable in systems with B^{4+}/A^{3+} size ratios comparable to or smaller than $Ho_2Zr_2O_7$ compounds, shows a more general trend for the increasing preference for higher oxygen coordination around the tetravalent (trivalent) cation as the size of B^{4+} increases (decreases) relative to A^{3+}. This general trend is consistent with previous experimental investigations on $RE_2Hf_2O_7$ and $RE_2Zr_2O_7$[29,30], which show that increasing size of the RE cation increases the preferred coordination around it. Overall, the results of the current study suggest that the weberite-type order reported by Shamblin *et al.*[20] in $Ho_2Zr_2O_7$ is expected to be energetically preferred in trivalent-substituted fluorite-oxide phases that have B^{4+}/A^{3+} size ratios intermediate between the smaller values characteristic of pyrochlore ordering and the larger values associated with the $RE_2Th_2O_7$ systems considered here.

Methods

The computational approach employed in this work is designed to understand trends in the ordering of the tetravalent and trivalent cations and oxygen vacancies across the range of chemistries for the $A_2B_2O_7$ systems considered. These trends in preferred ordering motifs are investigated through the consideration of a set of hypothetical long-range-ordered fluorite superstructures, designed to probe different coordinations of oxygen and vacancies around the trivalent and tetravalent cations, as well as different cation ordering patterns. The energetic driving forces associated with these different ordering motifs are investigated by comparing the energies of the hypothetical long-range-ordered phases with a random solid-solution phase modeled with SQS structures, as described in the main text. We note that this approach cannot be used to fully describe the state of short-range order present in the experimental samples, including in particular the spatial range of the short-range-ordered domains. Rather, the goal is to understand the energetics underlying the formation of such short-range order, as well as the energetically preferred anion and cation ordering configurations. In this approach, the formation energies of relaxed structures were obtained using DFT within the formalism of the projector augmented-wave (PAW) method[35,36] and the Perdew-Burke-Ernzerhof (PBE) generalized gradient approximation (GGA)[37,38], as implemented in the Vienna *ab initio* simulation package (VASP)[39,40]. The PAW potentials use 4 valence electrons for Zr ($5s^24d^2$), 12 for Th ($6s^26p^66d^27s^2$), 11 for Y ($4s^24p^65s^24d^1$) and La ($5s^25p^66s^25d^1$) and 6 for O ($2s^22p^4$). For Ho, Gd, and Nd, the occupied 4*f* orbitals in the trivalent oxidation state are treated as core electrons. We employ a plane-wave cutoff energy of 400 eV and 500 eV for $Ho_2Zr_2O_7$ and $RE_2Th_2O_7$, respectively, and the Brillouin zone is sampled using the Monkhorst-Pack scheme with relatively coarse k-point meshes of at least $4 \times 4 \times 4$ and $1 \times 2 \times 2$ for the $A_2B_2O_7$-fluorite and weberite-type structures, respectively, to initially screen out energetically disfavorable structures. The lowest energy $Ho_2Zr_2O_7$ structures were then sampled with k-point meshes of $8 \times 8 \times 8$ and $4 \times 4 \times 4$ for the $A_2B_2O_7$-fluorite and weberite-type structures, respectively. In the $RE_2Th_2O_7$ systems, k-points meshes of $4 \times 4 \times 4$ were found to be sufficient to achieve well converged energies. The k-point meshes used for the end members for the formation energy calculations are $8 \times 8 \times 8$ for cubic ZrO_2, $6 \times 6 \times 6$ for cubic ThO_2, $4 \times 4 \times 4$ for C-type Ho_2O_3, Y_2O_3, and Gd_2O_3, and $8 \times 8 \times 8$ for A-type Nd_2O_3 and La_2O_3. From convergence checks with respect to plane-wave cutoff and k-point sampling, the energy differences between low energy structures are estimated to be converged to within 0.3 kJ/mol-cation. Electronic self-consistency was considered achieved when

the total energy change between electronic steps is within 10^{-4} eV, and relaxation of ionic positions and cell shape were carried out with no symmetry constraints until residual forces were below approximately 15 meV/Å.

References

1. Subramanian, M. A., Aravamudan, G. & Subba Rao, G. V. Oxide pyrochlores — A review. *Progress in Solid State Chemistry* **15,** 55–143 (1983).
2. Scott, H. G. The yttria-zirconia δ phase. *Acta Crystallographica Section B* **33,** 281–282 (1977).
3. Minervini, Licia., Grimes, R. W. & Sickafus, K. E. Disorder in Pyrochlore Oxides. *Journal of the American Ceramic Society* **83,** 1873–1878 (2000).
4. Lee, T. A., Navrotsky, A. & Molodetsky, I. Enthalpy of formation of cubic yttria-stabilized zirconia. *Journal of Materials Research* **18,** 908–918 (2003).
5. Vanpoucke, D. E. P., Bultinck, P., Cottenier, S., Van Speybroeck, V. & Van Driessche, I. Density functional theory study of $La_2Ce_2O_7$: disordered fluorite versus pyrochlore structure. *Phys. Rev. B* **84,** 054110 (2011).
6. Burbano, M. *et al.* Oxygen vacancy ordering and the conductivity maximum in Y_2O_3-doped CeO_2. *Chemistry of Materials* **24,** 222–229 (2012).
7. Norberg, S. T. *et al.* Pyrochlore to fluorite transition: The $Y_2(Ti_{1-x}Zr_x)_2O_7$ ($0.0 \leq x \leq 1.0$) system. *Chemistry of Materials* **24,** 4294–4300 (2012).
8. Navrotsky, A. Thermodynamics of solid electrolytes and related oxide ceramics based on the fluorite structure. *J. Mater. Chem.* **20,** 10577–10587 (2010).
9. Busker, G., Chroneos, A., Grimes, R. W. & Chen, I.-W. Solution mechanisms for dopant oxides in yttria. *Journal of the American Ceramic Society* **82,** 1553–1559 (1999).
10. Minervini, L., Zacate, M. O. & Grimes, R. W. Defect cluster formation in M_2O_3-doped CeO_2. *Solid State Ionics* **116,** 339–349 (1999).
11. Bogicevic, A., Wolverton, C., Crosbie, G. M. & Stechel, E. B. Defect ordering in aliovalently doped cubic zirconia from first principles. *Phys. Rev. B* **64,** 014106 (2001).
12. Bogicevic, A. & Wolverton, C. Nature and strength of defect interactions in cubic stabilized zirconia. *Phys. Rev. B* **67,** 024106 (2003).
13. Predith, A., Ceder, G., Wolverton, C., Persson, K. & Mueller, T. *Ab initio* prediction of ordered ground-state structures in ZrO_2–Y_2O_3. *Phys. Rev. B* **77,** 144104 (2008).
14. Middleburgh, S. *et al.* Solution of trivalent cations into uranium dioxide. *Journal of Nuclear Materials* **420,** 258–261 (2012).
15. Alexandrov, V., Grønbech-Jensen, N., Navrotsky, A. & Asta, M. First-principles computational study of defect clustering in solid solutions of ThO_2 with trivalent oxides. *Phys. Rev. B* **82,** 174115 (2010).
16. Solomon, J., Navrotsky, A. & Asta, M. Energetics and defect clustering trends for trivalent rare earth cations substituted in UO_2. *Journal of Nuclear Materials* **457,** 252–255 (2015).
17. Inaba, H. & Tagawa, H. Ceria-based solid electrolytes. *Solid State Ionics* **83,** 1–16 (1996).
18. He, H., Keech, P. G., Broczkowski, M. E., Noel, J. J. & Shoesmith, D. W. Characterization of the influence of fission product doping on the anodic reactivity of uranium dioxide. *Canadian Journal of Chemistry* **85,** 702–713 (2007).
19. Razdan, M. & Shoesmith, D. W. Influence of Trivalent-Dopants on the Structural and Electrochemical Properties of Uranium Dioxide (UO_2). *Journal of The Electrochemical Society* **161,** H105–H113 (2014).
20. Shamblin, J. *et al.* Probing disorder in isometric pyrochlore and related complex oxides. *Nat Mater* **15,** 507–511 (2016).
21. Stanek, C. R. *et al.* Predicted structure and stability of $A_4B_3O_{12}$ δ-phase compositions. *Phys. Rev. B* **80,** 174101 (2009).
22. Aizenshtein, M., Shvareva, T. Y. & Navrotsky, A. Thermochemistry of lanthana- and yttria-doped thoria. *Journal of the American Ceramic Society* **93,** 4142–4147 (2010).
23. Hart, G. L. W. & Forcade, R. W. Algorithm for generating derivative structures. *Phys. Rev. B* **77,** 224115 (2008).
24. van de Walle, A., Asta, M. & Ceder, G. The alloy theoretic automated toolkit: A user guide. *Calphad* **26,** 539–553 (2002).
25. van de Walle, A. Multicomponent multisublattice alloys, nonconfigurational entropy and other additions to the alloy theoretic automated toolkit. *Calphad* **33,** 266–278 (2009).
26. Zunger, A., Wei, S. H., Ferreira, L. G. & Bernard, J. E. Special quasirandom structures. *Phys. Rev. Lett.* **65,** 353–356 (1990).
27. Jiang, C., Stanek, C. R., Sickafus, K. E. & Uberuaga, B. P. First-principles prediction of disordering tendencies in pyrochlore oxides. *Phys. Rev. B* **79,** 104203 (2009).
28. Wolff-Goodrich, S., Hanken, B. E., Solomon, J. M. & Asta, M. Special quasirandom structure modeling of fluorite-structured oxide solid solutions with aliovalent cation substitutions. *Modelling and Simulation in Materials Science and Engineering* **23,** 055001 (2015).
29. Blanchard, P. E. *et al.* Does local disorder occur in the pyrochlore zirconates? *Inorganic Chemistry* **51,** 13237 (2012).
30. Blanchard, P. E. *et al.* Investigating the local structure of lanthanoid hafnates $Ln_2Hf_2O_7$ via diffraction and spectroscopy. *The Journal of Physical Chemistry C* **117,** 2266–2273 (2013).
31. Sanjuán, M. L. *et al.* Raman and x-ray absorption spectroscopy study of the phase evolution induced by mechanical milling and thermal treatments in $R_2Ti_2O_7$ pyrochlores. *American Physical Society* 84, 104207 (2013).
32. Zhang, L., Solomon, J. M., Asta, M. & Navrotsky, A. A combined calorimetric and computational study of the energetics of rare earth substituted UO_2 systems. *Acta Materialia* **97,** 191–198 (2015).
33. Cowley, J. M. An approximate theory of order in alloys. *Phys. Rev*. **77,** 669–675 (1950).
34. Shannon, R. D. Revised effective ionic radii and systematic studies of interatomic distances in halides and chalcogenides. *Acta Crystallographica Section A* **32,** 751–767 (1976).
35. Blöchl, P. E. Projector augmented-wave method. *Phys. Rev. B* **50,** 17953–17979 (1994).
36. Kresse, G. & Joubert, D. From ultrasoft pseudopotentials to the projector augmented-wave method. *Phys. Rev. B* **59,** 1758–1775 (1999).
37. Perdew, J. P., Burke, K. & Ernzerhof, M. Generalized gradient approximation made simple. *Phys. Rev. Lett.* **77,** 3865–3868 (1996).
38. Perdew, J. P., Burke, K. & Ernzerhof, M. Generalized gradient approximation made simple. *Phys. Rev. Lett.* **78,** 1396–1396 (1997).
39. Kresse, G. & Furthmüller, J. Efficient iterative schemes for *ab initio* total-energy calculations using a plane-wave basis set. *Phys. Rev. B* **54,** 11169–11186 (1996).
40. Kresse, G. & Furthmüller, J. Efficiency of ab-initio total energy calculations for metals and semiconductors using a plane-wave basis set. *Computational Materials Science* **6,** 15–50 (1996).

Acknowledgements

This work was supported by the Office of Basic Energy Sciences of the U.S. Department of Energy as part of the Materials Science of Actinides Energy Frontier Research Center (DE-SC0001089). This work made use of resources of the National Energy Research Scientific Computing Center, supported by the Office of Basic Energy Sciences of the U.S. Dept of Energy (DE-AC02-05CH11231).

Author Contributions

The computational study was conceived by all of the authors. All computations were performed by J.M.S. The results were analyzed by J.M.S. with input from all of the authors. Each of the authors contributed to the writing and review of the manuscript.

Additional Information

Competing financial interests: The authors declare no competing financial interests.

How to cite this article: Solomon, J. M. *et al.* Chemical ordering in substituted fluorite oxides: a computational investigation of $Ho_2Zr_2O_7$ and $RE_2Th_2O_7$ (RE=Ho, Y, Gd, Nd, La). *Sci. Rep.* **6**, 38772; doi: 10.1038/srep38772 (2016).

Publisher's note: Springer Nature remains neutral with regard to jurisdictional claims in published maps and institutional affiliations.

SCIENTIFIC REPORTS

OPEN

Corrigendum: Chemical ordering in substituted fluorite oxides: a computational investigation of $Ho_2Zr_2O_7$ and $RE_2Th_2O_7$ (RE = Ho, Y, Gd, Nd, La)

Jonathan M. Solomon, Jacob Shamblin, Maik Lang, Alexandra Navrotsky & Mark Asta

Scientific Reports **6**:38772; doi: 10.1038/srep38772; published online 12 December 2016; updated on 13 February 2017

This Article contains errors in Reference 31 which was incorrectly given as:

'Sanjuán, M. L. *et al.* Raman and x-ray absorption spectroscopy study of the phase evolution induced by mechanical milling and thermal treatments in R2Ti2O7 pyrochlores. *American Physical Society* **84**, 104207 (2013)'.

The correct reference is listed below:

Sanjuán, M. L. *et al.* Raman and x-ray absorption spectroscopy study of the phase evolution induced by mechanical milling and thermal treatments in R2Ti2O7 pyrochlores. *Phys. Rev.* B **84**, 104207 (2011).